Supplementary Information for

High Resolution Mapping of Oxygen Reduction Reaction Kinetics at

Polycrystalline Platinum Electrodes

Chang-Hui Chen,[a] Katherine E. Meadows,[a] Anatolii Cuharuc,[a] Stanley C. S. Lai,[a,b] and Patrick R. Unwin[a,*]

[a] Department of Chemistry, University of Warwick, Gibbet Hill Rd, Coventry CV4 7AL, UK.

[b] MESA+ Institute for Nanotechnology, University of Twente, PO Box 217, 7500 AE Enschede, The Netherlands

[*] To whom correspondence should be addressed: P.R.Unwin@warwick.ac.uk

Contents

1. Cyclic voltammograms of oxygen reduction reaction (ORR)

2. Finite element method (FEM) modelling

3. Scanning electrochemical cell microscopy (SECCM) ion conductance current images

1. Cyclic voltammograms of oxygen reduction reaction (ORR)

Figure S1 shows cyclic voltammograms (CVs) of a polycrystalline Pt electrode recorded in aerated and nitrogen purged solutions. The experiment was performed in a conventional three electrode system using a piece of Pt wire (flame annealed) as the working electrode, with a Pd-H_2 and Pt wire as reference electrode and counter electrode, respectively. All the potentials reported are relative to reversible hydrogen electrode (RHE). The solution was deaerated by flowing nitrogen through 10 mL of 50 mM sulfuric acid solution for 30 min. Furthermore, a nitrogen flow was sustained over the solution during the CV measurement. As shown in Figure S1, the CV under deaerated conditions shows the characteristic features of a polycrystalline electrode in sulfuric acid solution.[1] After recording the CV, the solution was aerated for 1 h. The change in the CV morphology on the cathodic scan in this solution (red line) is due to the oxygen reduction reaction.
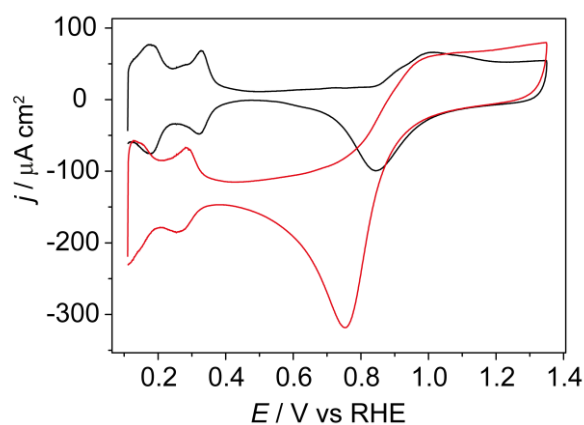
Figure S1. Cyclic voltammograms of platinum in nitrogen purged (black) and air saturated (red) 0.05 M sulfuric acid solutions at a scan speed of 50 mV s^{-1}.

2. Finite element method (FEM) modelling

The SECCM setup was modelled using COMSOL Multiphysics 4.3 (COMSOL AB, Sweden) as described in detail elsewhere.[2-4] Briefly, the concept of the model is as follows. The pipette and the electrolyte meniscus are considered as truncated cones, as shown in Figure S2. Although a 3D simulation is necessary, a plane of symmetry perpendicular to the theta pipette inner wall means that only half of the pipette needs to be considered, which improves the computational efficiency.[4] The dimensions of the pipette opening, defined by r_a and r_b, were obtained from a field emission-scanning electron microscope (FE-SEM) image of the pipette (see *main text*). The dimensions of the meniscus were also measured by FE-SEM, and showed major and minor semi axes, r_{ma} and r_{mb}, of 650 nm and 520 nm, respectively. For the simulation, we used a taper angle of the pipette of $\theta = 8°$, within the typical measured range of values.[4] Based on the average values of ion conductance current (12 nA) and the alternating current set point (200 pA), we determined the meniscus height, m_h, to be 150 nm, for the experiment where a kinetic analysis was carried out.
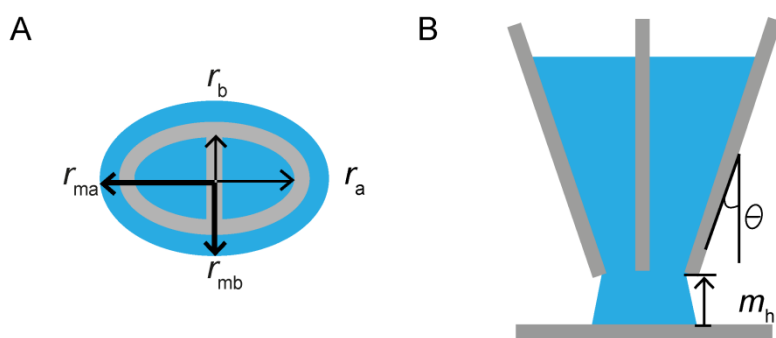
Figure S2. Schematics of the pipette (grey) and meniscus (blue) geometry used for FEM simulations. (A) r_a and r_b (thin arrows) represent the major and minor inner radius of the pipette; r_{ma} and r_{mb} (thick arrows) indicate the major and minor radius of the meniscus. (B) θ and m_h are the angle of the pipette and the height of the meniscus, respectively.

The model included four molecular species: H^+, SO_4^{2-}, HSO_4^- and O_2. The diffusion coefficients for all species and the molar conductivity values for the ions were obtained from literature and are summarized in Table S1.

Table S1: Values for the ionic conductivity and diffusion coefficients of solution species, with their source (reference in superscripts).

Species	Λ_j (S cm^2 mol^{-1})	D (10^{-5} cm^2 s^{-1})
H^+	349.65 [5]	7.90 [6]
HSO_4^-	52 [5]	1.39 [5]
1/2 SO_4^{2-}	80 [5]	1.07 [5]
O_2		2.1 [7]

The concentration of sulfuric acid was 50 mM. The speciation was evaluated with the known pK_a values of H_2SO_4 corrected for activity. The distribution of concentrations and the electric field in the pipette and meniscus were computed under steady-state conditions by solving the Nernst-Plank equation with electroneutrality. Due to the rapid gaseous O_2 transport[7] from air to the meniscus walls, we imposed a Dirichlet boundary conditions on the meniscus:

$$C_{O_2}(walls) = C_{O_2}^0 \qquad \text{(S1)}$$

where $C_{O_2}^0$ designates the concentration of oxygen in air-saturated solution (2.5×10^{-7} mol cm^{-3}).[7] This means that, besides the diffusion of O_2 down to the pipette, there is also a constant flux of O_2 from the meniscus "walls" (across the air/solution interface). Since we used the simulations mainly to investigate mass transport effects in the SECCM ORR experiment, we applied an effective rate constant for the ORR, k_r (variable), see equation S2. It was included in the model as a boundary condition at the electrode surface (equation S3 and S4). The faradaic current, i, was computed from equation S5.

$$O_2 + 4H^+ + 4e^- \xrightarrow{\ k_r\ } 2H_2O \qquad \text{(S2)}$$

$$J_{O_2} = -k_r C_{H^+} C_{O_2} \qquad \text{(S3)}$$

$$J_{O_2} = \frac{1}{4} J_{H^+} \qquad \text{(S4)}$$

$$i = 8F \int_\Omega D_{O_2} \left(\frac{\partial C_{O_2}}{\partial z} \right)_{z=0} dS \qquad \text{(S5)}$$

Here, the factor 8 results from the four electron reaction and the symmetry of the simulation mentioned above. The integration in equation S5 was performed over the surface of the meniscus contact area Ω. Other symbols have their usual meaning as described above and in reference 4.

By applying a range of reaction rate constants, k_r, at the surface and solving equations S3, S4 and S5, a working curve of electrochemical current (i) vs. k_r can be produced (Figure S3), together with a plot of proton concentration near the working electrode vs. i (see *main text*, Figure 6). By matching experimental i values, one can extract k_r and the proton concentration for a potential of interest. At 0.55 V, the average current across the entire scanned area is 8.6 pA, corresponding to a k_r of 9.0×10^{-3} cm s^{-1}. By applying the same kinetic analysis as in the main text, an exchange current density of 1.29 µA cm^{-2} was obtained. This value is close to the exchange current density (1.38 µA cm^{-2}) calculated from the experimental data, confirming the validity of the simulation.
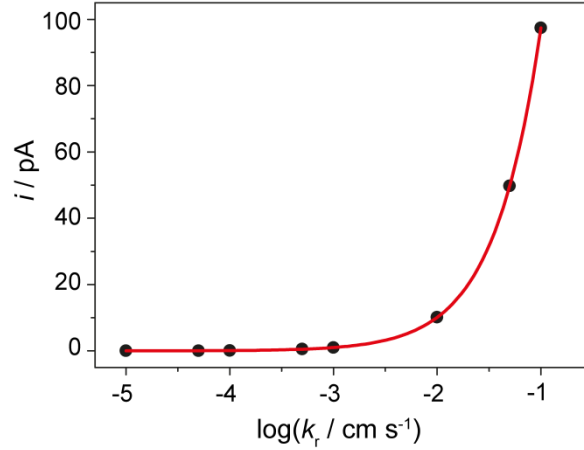
Figure S3. Working curve of electrochemical current vs. effective rate constant for the ORR. Geometric parameters are described in the text.

To further investigate the relative contributions of diffusion of O_2 down the barrels compared to that across the meniscus, a zero-flux boundary condition (equation S6) was applied on the meniscus "walls" and the limiting current was obtained by applying equation S7 on the working electrode surface.

$$J_{O_2}(walls) = 0 \tag{S6}$$

$$(C_{O_2})_{z=0} = 0 \tag{S7}$$

This leads to a value for the limiting current of 27 pA which is about one third of the limiting current obtained in SECCM imaging (see *main text*, Figure 3). This result clearly shows the impact of the meniscus in enhancing oxygen mass transport in the SECCM setup.

3. SECCM ion conductance current images

In addition to the electrochemical current images, the ion conductance current (i_{dc}) between the two quasi-reference counter electrodes (QRCEs), the corresponding ac component of the ion conductance current (i_{ac}), and the position of the piezoelectric positioners were recorded simultaneously during SECCM imaging.[2, 8, 9] Figures S4A and S4B show typical responses of i_{dc} and i_{ac} for the data in Figure 3A (see *main text*). The stable current maps demonstrate the stability of the meniscus size and the constancy of the pipette-substrate separation during scanning.[2, 3, 8, 10]
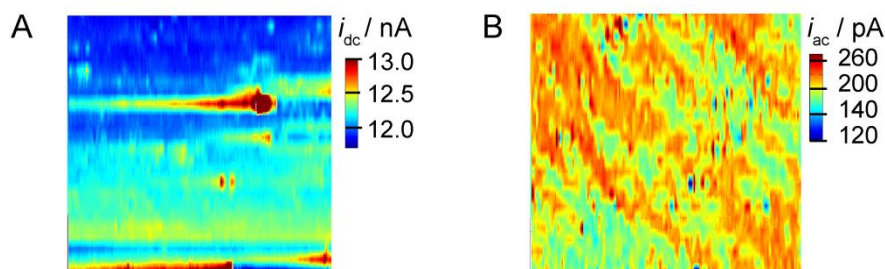
Figure S4. Typical SECCM ion conductance current (A) and ac component of the ion conductance current (B) image obtained while carrying out the ORR on a polycrystalline platinum electrode at 0.65 V vs. RHE.

References

1.　V. Climent and J. M. Feliu, *J. Solid State Electrochem.*, 2011, **15**, 1297-1315.
2.　A. G. Güell, N. Ebejer, M. E. Snowden, J. V. Macpherson and P. R. Unwin, *J. Am. Chem. Soc.*, 2012, **134**, 7258-7261.
3.　A. G. Güell, N. Ebejer, M. E. Snowden, K. McKelvey, J. V. Macpherson and P. R. Unwin, *Proc. Natl. Acad. Sci. USA*, 2012, **109**, 11487-11492.
4.　M. E. Snowden, A. G. Güell, S. C. S. Lai, K. McKelvey, N. Ebejer, M. A. O'Connell, A. W. Colburn and P. R. Unwin, *Anal. Chem.*, 2012, **84**, 2483-2491.
5.　D. R. Lide, ed., *CRC Handbook of Chemistry and Physics*, CRC Press, Boca Raton.
6.　J. V. Macpherson and P. R. Unwin, *Anal. Chem.*, 1997, **69**, 2063-2069.
7.　C. J. Slevin, S. Ryley, D. J. Walton and P. R. Unwin, *Langmuir*, 1998, **14**, 5331-5334.
8.　N. Ebejer, A. G. Güell, S. C. S. Lai, K. McKelvey, M. E. Snowden and P. R. Unwin, *Annu. Rev. Anal. Chem.*, 2013, **6**, 329-351.
9.　N. Ebejer, M. Schnippering, A. W. Colburn, M. A. Edwards and P. R. Unwin, *Anal. Chem.*, 2010, **82**, 9141-9145.
10.　S. C. S. Lai, A. N. Patel, K. McKelvey and P. R. Unwin, *Angew. Chem. Int. Ed.*, 2012, **51**, 5405-5408.